Performance Evaluation of Variable Structure and Linear Control Strategies for Grid Connected PMSG Wind Energy System under Different Operating Conditions

Youssef Errami[1], Abdellatif Obbadi[1], Smail Sahnoun[1], Mohammed Ouassaid[2], and Mohamed Maaroufi[2]

[1]Laboratory: Electronics, Instrumentation and Energy- Team: Exploitation and Processing of Renewable Energy, Department of Physics, Faculty of Science, University Chouaib Doukkali, Eljadida, Morocco
[2]Department of Electrical Engineering, Mohammadia School's of Engineers,
Mohammed V University, Rabat, Morocco
errami.emi@gmail.com

Abstract: As the penetration of the Wind Energy Generation System (WEGS) into the modern power systems is extensively increased, an efficient control strategy of a WEGS plays an essential role in wind power utilization. This study presents Sliding Mode Control (SMC) design for the Variable Speed Wind Farm Systems (VS-WFS) based on Permanent Magnet Synchronous Generator (PMSG) and interconnected to the electric network. The proposed control laws are used to regulate both grid-side and generator converters. The generator side converters are used to track the maximum wind power. The function of the grid side inverter is to transfer the total extracted wind power from DC-link to the electric network and regulate the DC-link voltage. A SMC scheme is developed in the sense of Lyapunov stability theorem for the VS-WFS. Besides, the effectiveness of the proposed SMC scheme is demonstrated by comparison with a traditional Proportional Integral (PI) control strategy for fault conditions as well as for normal working conditions. Simulation results with Matlab/Simulink environment are presented to support the theoretical considerations demonstrating the potential contributions of both control strategies. The proposed SMC scheme can provide excellent control performance than the traditional PI strategy.

Keywords: Wind farm system, PMSG, MPPT, Variable-speed control, PFC control, Nonlinear Control, Sliding mode approach, Electric Network Connection.

1. Introduction

During the last few decades, with technological advancement, wind energy has grown rapidly and becomes the most competitive form of renewable energy systems [1]. Moreover, the most important aspect for connecting a Wind Farm System (WFS) with the electric network requires a power electronic converter that allows variable velocity operation, reduces both wind-energy cost and mechanical stress and increases reliability of system [2-3]. Then, operation at an optimum speed in response to wind velocity minimizes fluctuations of power output and their effects on the power distribution network. For this reason, variable speed WFS has attracted considerable attention around the world [4]. On the other hand, with the increased penetration of WFS into energy generation systems all over the world, Wind Turbine Generators (WTGs) based on Permanent Magnet Synchronous Generators (PMSG) are becoming popular for variable velocity power system and the use of the PMSG in large WTGs is growing quickly [5]. It is connected directly to the turbine without system of gearbox and so it can operate at low velocities. Moreover, this generator can reduce again weight, losses, costs, demands maintenance requirements [6]. Also, with the advance of power electronic technology, the wind farm systems are at present required to participate actively in distribution network system operation by appropriate generation control methodologies [7-8]. Furthermore, variable speed operation of Wind Energy Conversion System (WECS) is mandatory in order to adjust the rotational velocity of PMSG. Then, for various wind velocities, the WECS can be

Received: January 5th, 2015. Accepted: June 17th, 2016
DOI: 10.15676/ijeei.2016.8.2.13

operated in the Maximum Power Point Tracking (MPPT) strategy to extract the maximum wind power by adjusting the shaft velocity [9-10]. On the other hand, power electronic devices play a significant function in integration of WECS into an electrical network. They are generally adopted as the interface between the WECS and the power grid to give the ease for integrating the WECS units to reach high performance and effectiveness when connected to the electrical network [11]. The power electronic devices are used to control the speed of wind turbine, to decouple the PMSG from the power grid and the WECS does not need to synchronize its rotational velocity with the electrical network frequency [12]. It is important to note that it is fundamental to confine the converted mechanical power during high wind velocities and if the turbine extracted power reaches the nominal power [13-14]. Then, power limitation can be realized either by pitch control, stall control or active stall system. Diverse power conversion interfaces were presented in the literature for WECS based PMSG [15-23]. Figure 1 depicts the typical structure of WECS. It consists of a PMSG side rectifier and a grid side inverter interconnected through a dc-link system. The rectifier is used to control the power, the torque or the speed for PMSG. The capacitor decoupling allows the opportunity of separate control for each power electronic system. The task of the inverter is to synchronize the ac power generated by the WECS with the electrical network and to remain the dc-link voltage constant. Moreover, the inverter ought to have the aptitude of adjusting reactive and active power that the WECS exchange with the electric network and reach Unity Power Factor (UPF) of system. Furthermore, with a growing penetration of WECS in the modern electric network, it is mandatory that these systems should also be able to work under irregular and grid disturbances, correspondingly to the IEEE standards and the new grid codes [24]. As a result, the power quality from WECS creates significant defies for control strategies of power generation systems [24]. In recent studies, various control methods have been proposed for the operation of the grid side and the generator side. Conventional design methods of WECS control are

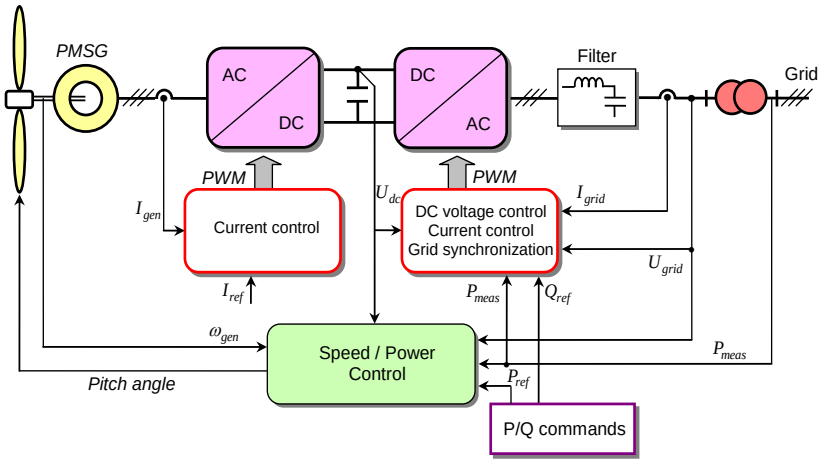

Figure 1. Typical structure of WECS connected to an electric network

based on Vector Control (VC) using d–q decoupling strategy and Proportional Integral (PI) regulators [19-23]. It is a linear method which is in general adjusted for a particular functional point of the WECS. Consequently, the performance of this control is significantly relies on the tuning of the system parameters. Also, it needs suitable decoupling, necessitates complex rotary transformation and several loops in the regulator. This will deteriorate the transient performance of VC and influence the stability of system within varying operating conditions. To surmount the drawbacks of VC, direct control methods such as Direct Power Control (DPC) and Direct Torque Control (DTC) were proposed lately [25-30]. The direct control approaches are distinguished by fast dynamic response, robustness against the WECS parameters variation,

simple structure, no coordinate transformation and enhanced dynamic performance. But, its performance deteriorates during very low velocity condition and at stable state there are significant ripples in flux /torque or active /reactive powers. Furthermore, the switching frequency is variable with operating point due to the utilization of predefined switching table and hysteresis regulator of WECS. On the other hand, for WECS integration into power grid and to overcome the abovementioned problems, there is the study of novel control approaches which must cope with the effects of the parameter variations of WECS, the nonlinear behavior of the system, typical uncertainties in both the electrical and the aerodynamic models, diverse external perturbations and the random variations of wind velocity [31]. Particularly, Sliding Mode Control (SMC) is a popular strategy due to the fact that it offers a numerous good properties, such as external disturbance rejection, fast dynamic response, high dynamic performance against unmodelled dynamics and low sensitiveness with respect to uncertainty [32-35]. Consequently, SMC is appropriate for wind power system applications. [36-38] propose the use of SMC approach to maximize the energy production of a WECS. [39-40] propose a pitch control based siding mode strategy to regulate the extracted power above the rated wind velocity. Sliding mode regulator to control the WECS for fault conditions is discussed in [41]. [42-43] use a SMC strategy of power converters.

In this context, this paper proposes a Variable Speed Wind Farm System (VS-WFS) based on the PMSG. The block diagram of proposed WFS is depicted in Figure 2. The system consists of 3 PMSGs connected to a common DC-bus system. Each PMSG of the VS-WFS is connected to the DC-bus through a rectifier. Therefore, velocity controllers are used so as to maximize the extracted energy from the wind, below the rated power area, while the control objectives of grid-side inverter system are to deliver the energy from the PMSG sides to the electrical network, to regulate the DC-link system voltage and to achieve Unity Power Factor (UPF) of VS-WFS.

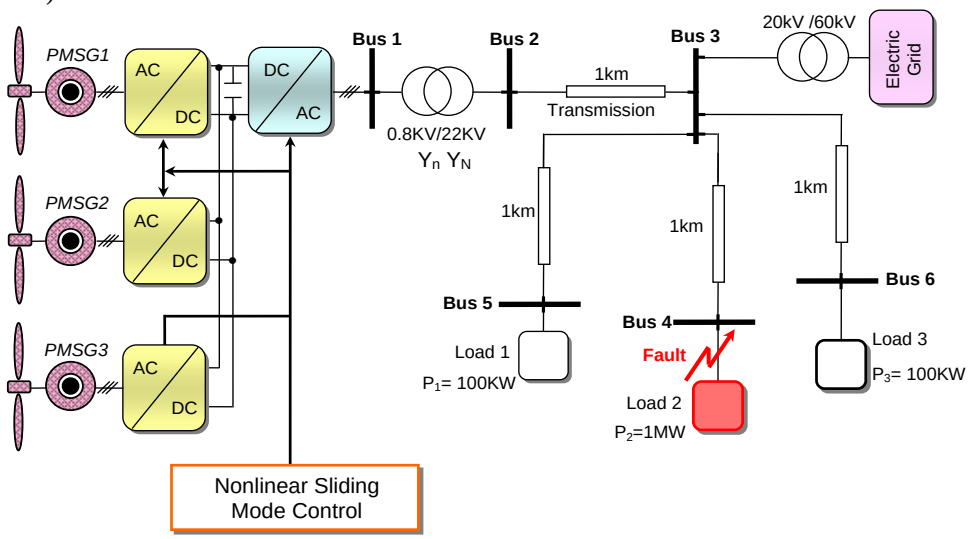

Figure 2. Configuration of the system.

Besides, VS-WFS has strong nonlinear multivariable with many uncertain factors and disturbances. For these reasons, SMC approach is used to achieve optimal control of the VS-WFS and the stability of the regulators is guaranteed using Lyapunov analysis. The aim of the control approach is to maximize the extracted power with the lowest possible impact in the utility grid frequency and voltage for fault conditions as well as for normal working conditions. On the other hand, a pitch control scheme for WFS is proposed to prevent wind turbines damage from excessive wind velocity. Also, system responses with the proposed SMC method are validated via simulations results and compared with those of conventional Vector Control (VC) based Proportional Integral (PI) controller systems.

The remainder of this paper is organized as follows. In Section 2, the model of the WFS is developed. In Section 3, SMC of the wind farm system will be presented. The simulations results are presented and analyzed in Section 4. In Section 5, some conclusions are given. References are provided in Section 6. Finally, Section 7 presents the parameters of the system under study.

2. Mathematical model of individual wind turbine generator

A. Wind Turbine Model

The mathematical relation for the mechanical power extracted from a variable velocity Wind Turbine (WT) is expressed as [44]:

$$P_{Turbine} = \frac{1}{2}\rho S C_P(\lambda,\beta) v^3 \tag{1}$$

where, ρ is the air density (typically 1.225 kg/m^3), S is the area swept by the rotor blades (in m^2), C_P is the coefficient of power conversion and v is the wind velocity (in m/s). The tip-speed ratio λ is given by [45]:

$$\lambda = \frac{\omega_m R}{v} \tag{2}$$

where R and ω_m are the rotor radium (in m) and rotor angular velocity (in rad/sec), respectively. The wind turbine mechanical torque output T_m given as:

$$T_m = \frac{1}{2}\rho S C_P(\lambda,\beta) v^3 \frac{1}{\omega_m} \tag{3}$$

The power coefficient is a nonlinear function of the tip-speed ratio λ and the blade pitch angle β (in degrees). Also, a generic equation is used to model the power coefficient $C_P(\lambda,\beta)$ based on the modeling turbine system characteristics described in [45] as:

$$C_P = \frac{1}{2}\left(\frac{116}{\lambda_i} - 0.4\beta - 5\right)e^{-\left(\frac{21}{\lambda_i}\right)}$$
$$\frac{1}{\lambda_i} = \frac{1}{\lambda + 0.08\beta} - \frac{0.035}{\beta^3 + 1} \tag{4}$$

The $C_P(\lambda,\beta)$ characteristics, for various values of the pitch angle β, are shown in Figure 3. The maximum value of C_P, that is $C_{P\max} = 0.41$, is achieved with $\beta = 0$ and with $\lambda_{opt} = 8.1$. Hence, in order to fully exploit the wind power, λ should be maintained at λ_{opt}, which is determined from the blade system design. The particular value λ_{opt} results in the point of optimal efficiency where the maximum power is captured by the WT system. For each wind velocity, there exists a specific point in the wind system power characteristic, MPPT, where the extracted power is maximized. Accordingly, the control methodology of the WFS load results in a variable velocity operation of the turbine system. So, the maximum power is generated continuously from the wind (MPPT control algorithm) [46]. That is illustrated in Figure 4.

B. Modeling of PMSG

In the synchronous d–q coordinates, the voltage equations of the PMSG are expressed as [45]:

$$v_{gq} = \left(R_g + p.L_q\right).i_q + \omega_e L_d i_d + \omega_e \psi_f \tag{5}$$

$$v_{gd} = \left(R_g + pL_d\right)i_d - \omega_e L_q i_q \tag{6}$$

where v_{gd} and v_{gq} are the direct stator and quadrature stator voltage, respectively. i_d and i_q are the direct stator and quadrature stator current, respectively. R_g is the stator resistance, L_q and L_d are the inductances of the generator on the q and d axis, ψ_f is the permanent magnetic flux and ω_e is the electrical rotating velocity of the PMSG, defined by:

$$\omega_e = p_n \omega_m \tag{7}$$

where p_n is the number of pole pairs of the generator and ω_m is the mechanical angular velocity.

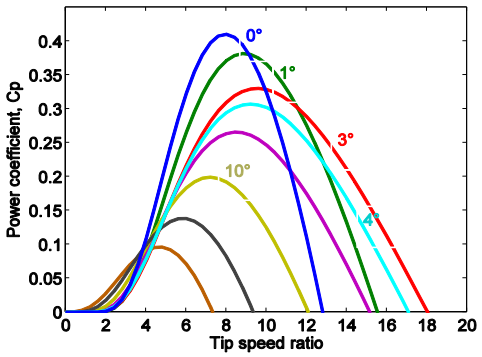

Figure 3. Characteristics C_p vs. λ ; for various values of the pitch angle β

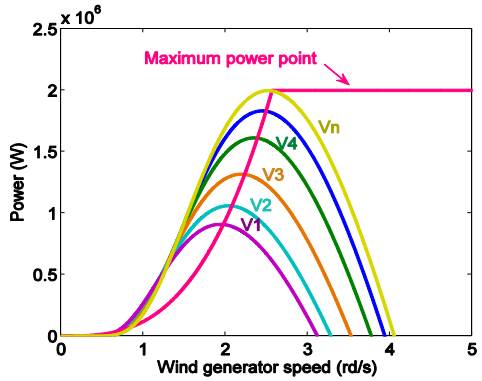

Figure 4. Wind generator power curves at various wind speed

If the PMSG is assumed to have equal q-axis, d-axis in inductances ($L_q = L_d = L_s$), the expression for the electromagnetic torque of generator can be described as:

$$T_e = \frac{3}{2} p_n \left[\psi_f i_q \right] \tag{8}$$

The dynamic equation of the wind turbine system is described by:

$$J \frac{d\omega_m}{dt} = T_e - T_m - F\omega_m \tag{9}$$

where J is the moment of inertia, F is the viscous friction coefficient and T_m is the mechanical torque developed by the Wind Turbine (WT).

3. The proposed control methodology of WFS

A. Maximum Power Point Tracking (MPPT) and Pitch Control system

Optimal operation of the WFS is to extract the maximum power from wind. In variable velocity WTGs, the speeds of the PMSGs are varied to achieve maximum coefficient of performance for the turbine systems. Therefore, optimal control algorithm of the system means that it has to track the optimum value of the shaft rotational velocity. Hence, the MPPT controller structure is used to generate the reference speed command of system. For any particular wind velocity, the turbine is capable to operate at the maximum power line as shown in Figure 4. In addition, it should always operate at λ_{opt}. As a result, the optimum rotational velocity of the wind turbine system can be simply estimated as follows:

$$\omega_{m-opt} = \frac{v\lambda_{opt}}{R} \tag{10}$$

ω_{m-opt} is the reference velocity, of the generator, which when applied to the velocity control loop of the PMSG side converter control system, maximum power will be produced by the WTG. So, the maximum mechanical extracted power of the turbine system is given as follows:

$$P_{Turbine\_\max i} = \frac{1}{2}\rho A C_{P\max}\left(\frac{R\omega_{m-opt}}{\lambda_{opt}}\right)^3 \tag{11}$$

Consequently, we can get the maximum power $P_{Turbine\_\max i}$ by regulating the PMSG velocity in different wind speed under rated power of the WFS. Moreover, the pitch angle controller is used in order to prevent WT damage from excessive wind velocity. The active power output is controlled based on the velocity of rotor. Once maximum rating of the power PMSG is reached in high wind velocities, the pitch angle is increased so as to shed the aerodynamic power and the wind turbine system operates at lower efficiency. Therefore, by reducing the coefficient of power conversion, both the power and rated rotor velocity are maintained for above rated wind speeds of WFS. The schematic diagram of pitch angle controller model is shown in Figure 5 where P_{ge} is the extracted power of the turbine system.

B. Variable structure control strategy for generator side converters with sliding mode control approach and MPPT

For each PMSG, the generator side three-phase converter is used as a rectifier with a Sliding Mode Variable Structure Control (SM-VSC). It works as a driver controlling the

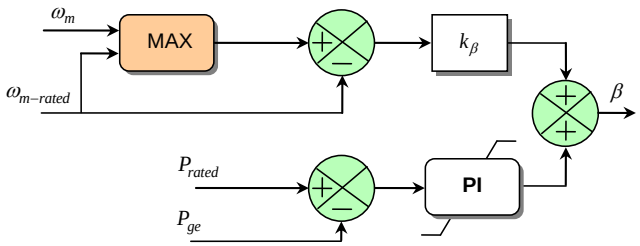

Figure 5. WFS pitch angle controller

generator operating at optimum generator velocity ω_{m-opt} in order to obtain MPPT from wind [46]. Besides, it is deduced from equations (8) and (9) that the WT speed can be controlled by regulating the q-axis stator current component (i_{qr}). As a result, the control diagram for individual generator-side converter system is shown as Figure 6.

In order to satisfy the sliding mode algorithm condition, it is necessary to define the sliding mode surface for the speed controller:

$$S_\omega = \omega_{m-opt} - \omega_m \tag{12}$$

ω_{m_opt} is generated by a MPPT strategy.

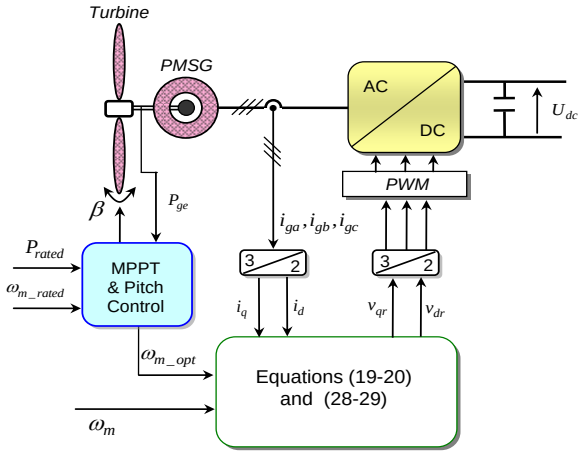

Figure 6. Individual PMSG side converter control diagram.

It follows that:

$$\frac{dS_\omega}{dt} = \frac{d\omega_{m\_opt}}{dt} - \frac{d\omega_m}{dt} \tag{13}$$

Combining (9) and (13) the following function is defined as:

$$\frac{dS_\omega}{dt} = \frac{d\omega_{m\_opt}}{dt} - \frac{1}{J}(T_e - T_m - F\omega_m) \tag{14}$$

Also, when the sliding mode algorithm occurs on the sliding mode surface [34]:

$$S_\omega = \frac{dS_\omega}{dt} = 0 \tag{15}$$

So, in order to obtain commutation around the surface with good dynamic performances, the control algorithm includes two terms [36]:

$$u_c = u_{eq} + u_n \tag{16}$$

u_{eq} is valid only in the sliding surface. During the sliding mode and in permanent regime, u_{eq} is calculated from (15), while u_n is used to guarantee the attractiveness of the variable to be controlled towards the commutation sliding mode control surface. Then:

$$u_n = \mu_\omega \operatorname{sgn}(S_\omega) \tag{17}$$

where $\mu_\omega \succ 0$.

On the other hand, SMC is a discontinuous control. So as to reduce the chattering, the continuous function as exposed in (18) where $\operatorname{sgn}(S_\omega)$ is a sign function defined as [78]:

$$\operatorname{sgn}(S_\omega) = \begin{cases} 1 & S_\omega \succ \varepsilon \\ \dfrac{S_\omega}{\varepsilon} & \varepsilon \geq |S_\omega| \\ -1 & -\varepsilon \succ S_\omega \end{cases} \tag{18}$$

ε is a small positive number. If the ε is too large or too small, the dynamic quality of the WFS will be reduced. Then, the value of ε should be chosen carefully.

Accordingly, so as to reduce the copper loss by setting the d axis current component to be zero and to ensure the PMSG velocity convergence to the optimum speed, references of currents components are derived. Then, the following equation for the system velocity is obtained from equations (12-16):

where $\mu_\omega \succ 0$.

Also, $i_{dr} = 0$ (19)

$$i_{qr} = \frac{2}{3 p_n \psi_f}(T_m + J\frac{d\omega_{m\_opt}}{dt} + F\omega_m + J\mu_\omega \operatorname{sgn}(S_\omega)) \quad (20)$$

$$S_\omega \frac{dS_\omega}{dt} = S_\omega \frac{d\omega_{m\_opt}}{dt} - \frac{S_\omega}{J}(T_e - T_m - F\omega_m)$$
$$= -\mu_\omega S_\omega \operatorname{sgn}(S_\omega) + \frac{S_\omega}{J}(T_m - \frac{3}{2} p_n \psi_f i_q + F\omega_m + J\mu_\omega \operatorname{sgn}(S_\omega) + J\frac{d\omega_{m\_opt}}{dt}) \quad (21)$$

On the other hand, SMC is used in order to regulate the currents components to their references. Let us introduce the following sliding surfaces for the current components i_d and i_q :

$$S_d = i_{dr} - i_d \quad (22)$$

$$S_q = i_{qr} - i_q \quad (23)$$

where i_{qr}, i_{dr} are the desired values of q-axis and d-axis current, respectively. So, it follows that:

$$\frac{dS_d}{dt} = \frac{di_{dr}}{dt} - \frac{di_d}{dt} = -\frac{1}{L_s}(v_{gd} - R_g i_d + L_s \omega_e i_q) \quad (24)$$

$$\frac{dS_q}{dt} = \frac{di_{qr}}{dt} - \frac{di_q}{dt} = \frac{di_{qr}}{dt} - \frac{1}{L_s}(v_{gq} - R_g i_q - L_s \omega_e i_d - \omega_e \psi_f) \quad (25)$$

when the sliding mode occurs on the sliding mode surfaces:

$$S_d = \frac{dS_d}{dt} = 0 \quad (26)$$

$$S_q = \frac{dS_q}{dt} = 0 \quad (27)$$

As a result, from equations (22-27), the control voltages of q axis and d axis are defined by:

$$v_{qr} = R_g i_q + L_s \omega_e i_d + \omega_e \psi_f + L_s \frac{di_{qr}}{dt} + L_s k_q \operatorname{sgn}(S_q) \quad (28)$$

$$v_{dr} = R_g i_d - L_s \omega_e i_q + L_s k_d \operatorname{sgn}(S_d) \quad (29)$$

where $k_q \succ 0$ and $k_d \succ 0$.

In addition, $S_d \frac{dS_d}{dt} = S_d\left[-\frac{1}{L_s}(v_{gd} - R_g i_d + L_s \omega_e i_q)\right]$ (30)

$$= -k_d S_d \operatorname{sgn}(S_d) + \frac{S_d}{L_s}\left[-v_{gd} + R_g i_d - L_s \omega_e i_q + L_s k_d \operatorname{sgn}(S_d)\right]$$

$$S_q \frac{dS_q}{dt} = S_q \left[\frac{di_{qr}}{dt} - \frac{di_q}{dt} \right] = -k_q S_q \operatorname{sgn}(S_q) + \frac{S_q}{L_s} \left[L_s \frac{di_{qr}}{dt} - v_{gq} + R_g i_q + L_s \omega_e i_d + \omega_e \psi_f + k_q L_s \operatorname{sgn}(S_q) \right] \tag{31}$$

Theorem 1: If the dynamic sliding mode algorithm laws are designed as (20), (28) and (29), therefore the global asymptotical stability of WFS is ensured.

Proof: To determine the required condition for the existence of the sliding mode control, it is fundamental to design the Lyapunov function. So, the following Lyapunov function is defined as :

$$\Upsilon_q = \frac{1}{2} S_\omega^2 + \frac{1}{2} S_q^2 + \frac{1}{2} S_d^2 \tag{32}$$

From Lyapunov stability techniques, to guarantee the attraction of the system throughout the sliding mode surface, Υ_q can be derived as:

$$\frac{d\Upsilon_q}{dt} \prec 0 \tag{33}$$

By differentiating the proposed Lyapunov function (32), we obtain:

$$\frac{d\Upsilon_q}{dt} = S_\omega \frac{dS_\omega}{dt} + S_d \frac{dS_d}{dt} + S_q \frac{dS_q}{dt} \tag{34}$$

Using (21) and (30-31) the following function is defined as:

$$\begin{aligned} \frac{d\Upsilon_q}{dt} = & -\mu_\omega S_\omega \operatorname{sgn}(S_\omega) + \frac{S_\omega}{J} (T_m - \frac{3}{2} p_n \psi_f i_q + F \omega_m + J \mu_\omega \operatorname{sgn}(S_\omega) + J \frac{d\omega_{m\_opt}}{dt}) \\ & - k_d S_d \operatorname{sgn}(S_d) + \frac{S_d}{L_s} \left[-v_{gd} + R_g i_d - L_s \omega_e i_q + L_s k_d \operatorname{sgn}(S_d) \right] \\ & - k_q S_q \operatorname{sgn}(S_q) + \frac{S_q}{L_s} \left[L_s \frac{di_{qr}}{dt} - v_{gq} + R_g i_q + L_s \omega_e i_d + \omega_e \psi_f + k_q L_s \operatorname{sgn}(S_q) \right] \end{aligned} \tag{35}$$

So, with (20), (28) and (29) the following equation is obtained:

$$\frac{d\Upsilon_q}{dt} = -\mu_\omega S_\omega \operatorname{sgn}(S_\omega) - k_d S_d \operatorname{sgn}(S_d) - k_q S_q \operatorname{sgn}(S_q) \tag{36}$$

Then, the following inequality is satisfied:

$$\frac{d\Upsilon_q}{dt} = -\mu_\omega |S_\omega| - k_d |S_d| - k_q |S_q| \prec 0 \tag{37}$$

Consequently, the global asymptotical stability is ensured and the velocity control tracking is achieved.

Finally, PWM is used in order to produce the control signal to implement the SMC for the generator side system. The double closed-loop control diagram for individual generator-side converter is shown as Figure 6.

C. Grid-side controller strategy with SMC

The structure of the wind farm system used for this study is shown in Figure7. It consists of 3 PMSGs based on 2MW generators connected to a common DC-bus. Each PMSG of the WFS system is connected to the DC-bus through a rectifier system, but the DC-bus is connected to the grid through only one DC/AC inverter. The grid-side converter is used in order to stabilize

the DC-link system voltage, to deliver the energy from the PMSGs sides to the electric network system and to set a UPF of WFS during wind variation. SMC is adopted to regulate the currents and output voltage in the inner control loops and the DC voltage controller in the second loop. Consequently, it can regulate instantaneous values of reactive power and active power of grid system connection, respectively.

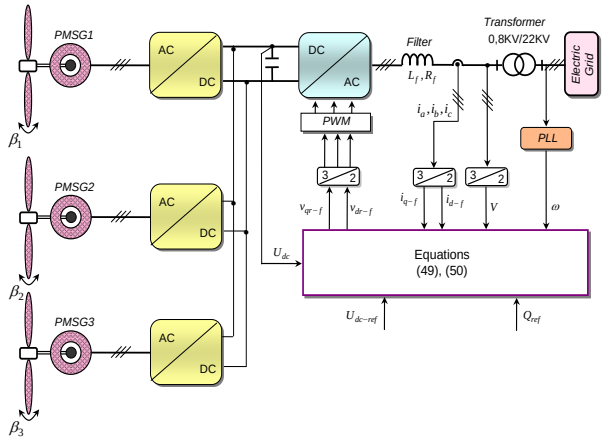

Figure 7. Schematic of control strategy for wind farm system

In the rotating dq reference frame, if the electric network system voltage space vector $\vec{u}$ is oriented on d-axis, then the voltage balance across the inductor L_f is given by [47]:

$$L_f \frac{di_{d-f}}{dt} = e_d - R_f i_{d-f} + L_f \omega i_{q-f} - V \tag{38}$$

$$L_f \frac{di_{q-f}}{dt} = e_q - R_f i_{q-f} - L_f \omega i_{d-f} \tag{39}$$

where L_f and R_f are the filter inductance and resistance respectively; e_q and e_d are the inverter q-axis and d-axis voltage components, respectively. i_{q-f}, i_{d-f} are the values of q-axis current and d-axis current, respectively. V is the grid system voltage component in the d-axis voltage component. In addition, the active power and reactive power can be given as follows:

$$P = \frac{3}{2} V i_{d-f} \tag{40}$$

$$Q = \frac{3}{2} V i_{q-f} \tag{41}$$

So, reactive power and active power control can be achieved by controlling direct and quadrature current components, respectively. Moreover, the DC-side equation can be given by [48]:

$$\frac{1}{2} C \frac{dU_{dc}^2}{dt} = P_{g\_t} - P \tag{42}$$

where P_{g_t} is the total output real power of generator stators. The d-axis reference current is determined by DC-link system voltage controller in order to control the converter output real power. For this reason, there are two closed-loop controls for the power converter. The fast dynamic loop is associated with the line current control in the inner loop where the SMC is adopted to track the line current control, but in the outer loop slow dynamic is associated with the dc bus system control. Also, the proportional integral (PI) linear controller is used so as to

generate the reference source current i_{dr-f} and regulate the dc voltage, but the reference signal of the q-axis current i_{qr-f} is created by the reactive power Q_{ref} according to (41).

Let us introduce the following sliding mode surfaces for the q- axis current and d-axis current:

$$S_{d-f} = i_{dr-f} - i_{d-f} \tag{43}$$

$$S_{q-f} = i_{qr-f} - i_{q-f} \tag{44}$$

where i_{qr-f}, i_{dr-f} are the desired values of q- axis current and d-axis current respectively. The reference i_{qr-f} for the i_{q-f} current is derived from the desired power factor. So:

$$\frac{dS_{d-f}}{dt} = \frac{di_{dr-f}}{dt} - \frac{di_{d-f}}{dt} = \frac{di_{dr-f}}{dt} - \frac{1}{L_f}(e_d - R_f i_{d-f} + L_f \omega i_{q-f} - V) \tag{45}$$

$$\frac{dS_{q-f}}{dt} = \frac{di_{qr-f}}{dt} - \frac{di_{q-f}}{dt} = \frac{di_{qr-f}}{dt} - \frac{1}{L_f}(e_q - R_f i_{q-f} - L_f \omega i_{d-f}) \tag{46}$$

when the sliding mode occurs on the sliding mode control surface, then:

$$S_{d-f} = \frac{dS_{d-f}}{dt} = 0 \tag{47}$$

$$S_{q-f} = \frac{dS_{q-f}}{dt} = 0 \tag{48}$$

Combining (38), (39) and (43)-(48) the control voltages of d axis and q axis are defined by:

$$v_{dr-f} = L_f \frac{di_{dr-f}}{dt} + R_f i_{d-f} - L_f \omega i_{q-f} + V + L_f k_{d-f} \operatorname{sgn}(S_{d-f}) \tag{49}$$

$$v_{qr-f} = R_f i_{q-f} + L_f \omega i_{d-f} + L_f k_{q-f} \operatorname{sgn}(S_{q-f}) \tag{50}$$

where $k_{d-f} \succ 0$ and $k_{q-f} \succ 0$.

In addition,

$$\begin{aligned} S_{d-f}\frac{dS_{d-f}}{dt} &= S_{d-f}\left[\frac{di_{dr-f}}{dt} - \frac{1}{L_f}(e_d - R_f i_{d-f} + L_f \omega i_{q-f} - V)\right] \\ &= -k_{d-f} S_{d-f} \operatorname{sgn}(S_{d-f}) \\ &\quad + \frac{S_{d-f}}{L_f}\left[L_f \frac{di_{dr-f}}{dt} - e_d + R_f i_{d-f} - L_f \omega i_{q-f} + V + k_{d-f} L_f \operatorname{sgn}(S_{d-f})\right] \end{aligned} \tag{51}$$

$$\begin{aligned} S_{q-f}\frac{dS_{q-f}}{dt} &= S_{q-f}\left[-\frac{di_{q-f}}{dt}\right] \\ &= -k_{q-f} S_{q-f} \operatorname{sgn}(S_{q-f}) + \frac{S_{q-f}}{L_f}\left[-e_q + R_f i_{q-f} + L_f \omega i_{d-f} + k_{q-f} L_f \operatorname{sgn}(S_{q-f})\right] \end{aligned} \tag{52}$$

Theorem 2: If the dynamic sliding mode algorithm laws are designed as (49) and (50) then the global asymptotical stability of system is ensured.

Proof: So as to determine the existence condition of the sliding mode control, it is required to design the Lyapunov function. Since, we can define a new function of Lyapunov including the q axis current and the d axis current as:

$$\Upsilon_f = \frac{1}{2} S_{d-f}^2 + \frac{1}{2} S_{q-f}^2 \tag{53}$$

From Lyapunov stability techniques, to guarantee the attraction of the system throughout the sliding mode surface and the sliding manifold is reached after a limited time, Υ_f can be derived as:

$$\frac{d\Upsilon_f}{dt} \prec 0 \tag{54}$$

By differentiating the Lyapunov function (53), we obtain:

$$\frac{d\Upsilon_f}{dt} = S_{d-f}\frac{dS_{d-f}}{dt} + S_{q-f}\frac{dS_{q-f}}{dt} \tag{55}$$

So, with (51) and (52):

$$\begin{aligned}\frac{d\Upsilon_f}{dt} &= -k_{d-f}S_{d-f}\,\mathrm{sgn}(S_{d-f}) \\ &+ \frac{S_{d-f}}{L_f}\left[L_f\frac{di_{dr-f}}{dt} - e_d + R_f i_{d-f} - L_f\omega i_{q-f} + V + k_{d-f}L_f\,\mathrm{sgn}(S_{d-f})\right] \\ &- k_{q-f}S_{q-f}\,\mathrm{sgn}(S_{q-f}) + \frac{S_{q-f}}{L_f}\left[-e_q + R_f i_{q-f} + L_f\omega i_{d-f} + k_{q-f}L_f\,\mathrm{sgn}(S_{q-f})\right]\end{aligned} \tag{56}$$

Combining (49) and (50) in (56) the following equation is obtained:

$$\frac{d\Upsilon_f}{dt} = -k_{d-f}S_{d-f}\,\mathrm{sgn}(S_{d-f}) - k_{q-f}S_{q-f}\,\mathrm{sgn}(S_{q-f}) \tag{57}$$

Then, the following inequality is satisfied:

$$\frac{d\Upsilon_f}{dt} = -k_{d-f}\left|S_{d-f}\right| - k_{q-f}\left|S_{q-f}\right| \prec 0 \tag{58}$$

Consequently, the asymptotic stability in the current loop is guaranteed and the dc-bus structure voltage control tracking is achieved. At last, PWM is used so as to produce the control signal. The configuration of the dc-link voltage and current controllers for grid-side converter is depicted in Figure 7.

4. Simulation and analysis

To verify the performance of the proposed control strategy, the simulation tests are implemented using Matlab/Simulink. This paragraph presents the simulated responses of the WFS under changing wind conditions and the grid system voltage dips conditions. In this example of simulation, it is used a variable speed WFS with a rated power of 6 MW. The farm consists of three 2MW wind turbine systems. The complete system was simulated by Matlab/Simulink using the parameters given in Table 1 and Table 2. During the simulation, for the PMSG side converter control systems, the d axis command current, i_{dr}, is set to zero; although, for the grid side inverter system, Q_{ref}, is set to zero. On the other hand, the DC-link voltage reference is fixed at $U_{dc-r} = 1900V$ and the electric network frequency value is steady at 50 Hz. The topology of the studied WFS based on PMSGs connected distribution network is depicted in Figure 2, Figure 6 and Figure 7. The grid voltage phase lock loop (PLL) system is implemented to track the fundamental phase and frequency. This section is divided into two parts, that is paragraph 4.1 demonstrates the acceptable performance of the WFS under varying wind conditions and normal working conditions, although paragraph 4.2 reflects the behavior of the WFS during the voltage dip. The simulation results are comparable with those in [12].

A. WFS characteristics under normal working conditions

The WFS response under SMC is illustrated by Figure 8-11. Figure 8a to Figure 8f show, respectively, the simulation results of instantaneous wind velocities, coefficients of power conversion C_p, pitch angles, rotors angular velocities of the PMSGs and total power generated. The rated wind speed considered in the simulation ($v_n = 12.4$ m/s). It can be seen, for each turbine system, the pitch control system is not active since the velocity never reaches the rated value (Figure 8(c)). At wind velocities below the rated speed area, the wind turbine controller maintains the coefficient of power at its maximum. The initial pitch angle β keeps the value of 0º and the power coefficient C_p is the maximum approximately $C_{P\max} = 0.41$(Figure 8(b)). The WFS operates under MPPT algorithm. At higher wind velocities, the coefficient of power diminishes to limit the rotor velocity. As shown in Figure 8(d), for high wind speeds at rated speed area, the mechanical angular velocities are saturated and constant. They have been limited by pitch control. The value of C_p are kept close to their optimal values in normal operation as illustrated in Figure 8(b). For each turbine, Cp is kept at the maximum value of 0.41 for a variable velocity region, but, if the wind speed reaches the rated wind velocity of the turbine systems (v_n =12.4 m/s), it is decreased according to the increase of the pitch angle as depicted in Figure 8(c). It can be seen, for each turbine system, that when the wind speeds increase, the rotor angular velocity increases proportionally too. Also, the pitch angle control method can limit, at high-wind-speed regions, the PMSG power and rotor velocity to their rated values (Figure 8(f) and Figure 8(d)). The total power generated of WFS is shown in Figure 8(f). The results show variation in the power extracted when the incoming wind speeds are different for each turbine system. Moreover, because all the turbines are working at their optimum level, and if the wind speeds are up the rated wind velocity, the total power generated reaches its maximum level (6MW). The PMSG2 speed is plotted in Figure 8(e), it follows its reference signal which depends on the wind speed and MPPT algorithm. Figure 8(e) shows that the mechanical angular velocity closely follows the optimum speed that is calculated from Eq. (10). The velocity regulation is such that it is difficult to discern any difference between the optimum speed and the actual mechanical speed. Notice this optimum speed is adjusted in response to the wind velocity changes to hold the maximum of coefficient of power conversion. It can be seen that, if the generator speed ω_m is higher than the rated speed $\omega_{m-rated}$ and the wind velocity is above the rated speed ($v_n = 12.4$ m/s), the pitch angle is activated to remove excessive power extracted from wind. Figure 9 shows the simulation result of reactive power of WFS. As can be seen, the wind farm supplies electric network system with a purely active power. Figure 10 shows the simulation result of dc link system voltage. The converter dc-link voltage is regulated constant at the reference value 1900 V. It can be observed that the grid-side regulator controls the dc-link voltage and the reactive power flow, and the generator side regulator controls the PMSG velocity. Figure 11 shows the variation and a closer observation of three phase voltage and current at Bus 1. The frequency is controlled and maintained at 50 Hz through a Phase Lock Loop (PLL) system. It is obvious that unity power factor of WFS is achieved approximatively and is independent of the variation of the wind velocity but only on the reactive power reference (Q_{ref}). It can be seen that the proposed strategy is efficient. This result further confirms the satisfactory working of the proposed control even for the variation of wind speed. Besides, simulations results and proposed strategy (Section 3) strongly agree and show good WFS performance.

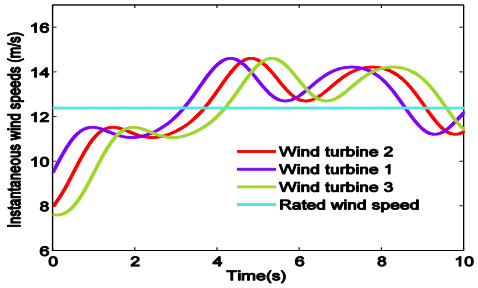

(a). Instantaneous wind speeds (m/s)

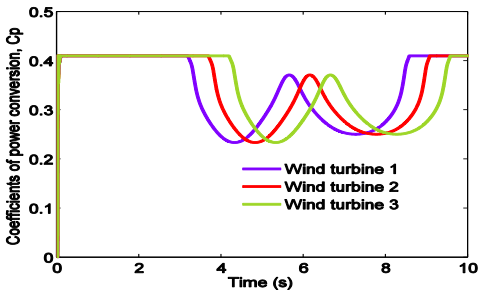

(b) *Coefficients of power conversion* C_p .

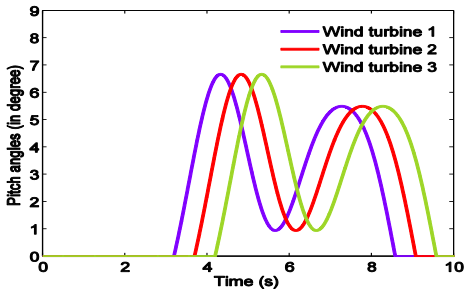

(c) Pitch angles β (in degree).

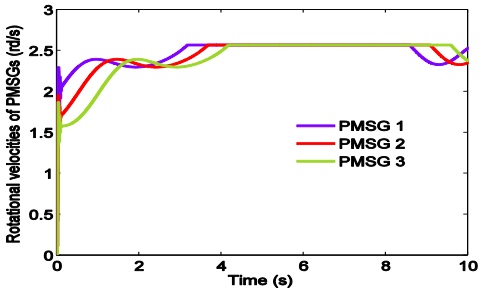

(d) *Rotors angular velocities of PMSGs*

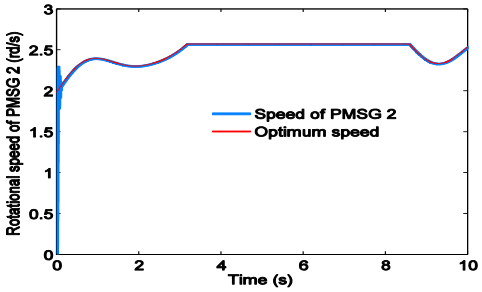

(e) *Speed of PMSG2 (rd/s).*

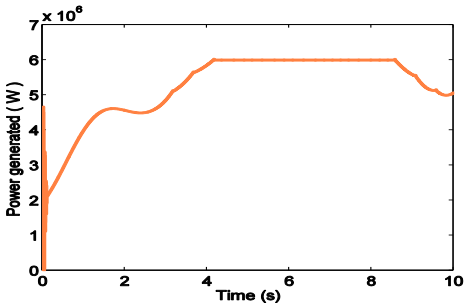

(f) *Total power generated.*

Figure 8. Waveforms of WFS characteristics with SMC.

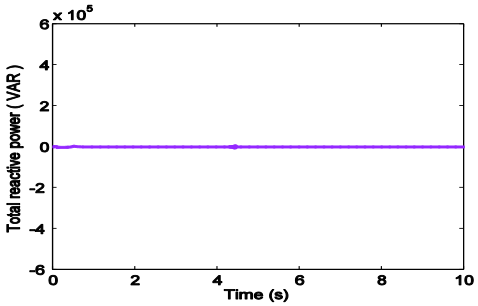

Figure 9. *Total reactive power (VAR).*

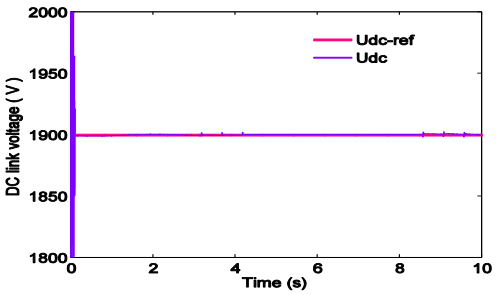

Figure 10. *DC link voltage (V).*

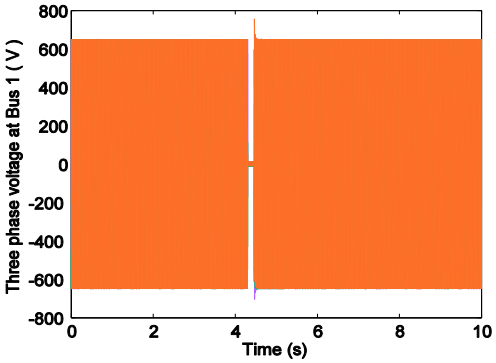

(a) Three phase voltage at Bus 1(V).

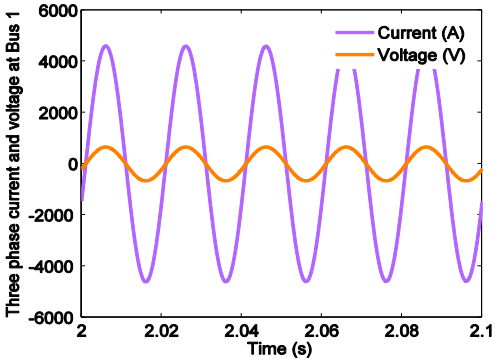

(b) Closer observation of three phase current and voltage at Bus 1.

Figure 11. Three phase current and voltage at Bus 1 for SMC

b) A performance comparison of a nonlinear and a linear control

In order to verify the performance of the proposed strategy based on the SMC approach, comparative simulation studies, involving conventional Proportional Integral (PI) linear controller, are presented. The proposed control strategy was compared against a reference [12]. To this aim, a series of simulations was carried out focusing on the velocity of PMSG, DC link voltage, three phase voltage and frequency performance. Figure 12 illustrates WFS response under conventional PI controller. Figure 13 and Figure 14 compare the system response for the proposed SMC and classic PI control, respectively. As shown in Figures 13a-e and Figure 13b-f, the transient responses of both dc link system voltage and speed of PMSGs for the SMC strategy are fast, while the dynamic response of the conventional PI control is largely dependent on the PI parameter controllers. Also, at transient state, the peaks of dc link voltage and velocity reach very high values with PI regulators than SMC. On the other hand, to demonstrate the pertinence of the proposed SMC approach, we test the performance of each controller under short circuit fault. So, the fault event is a three-phase to ground short-circuit fault,

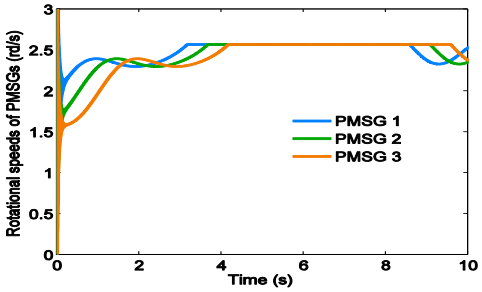

(a) *Rotors angular velocities of PMSGs (rd/s).*

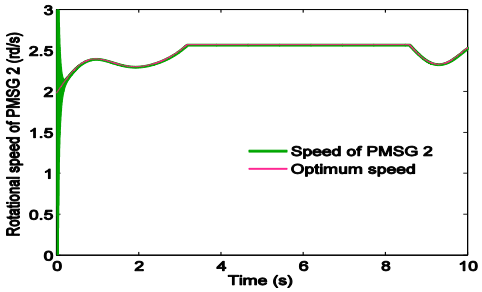

(b) *Speed of PMSG2 (rd/s).*

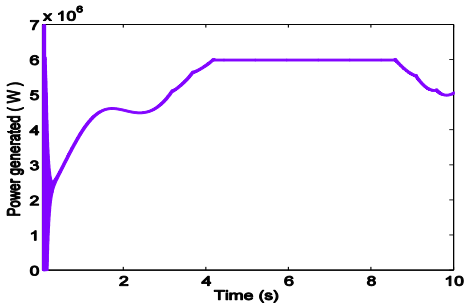

(c) *Total power generated.*

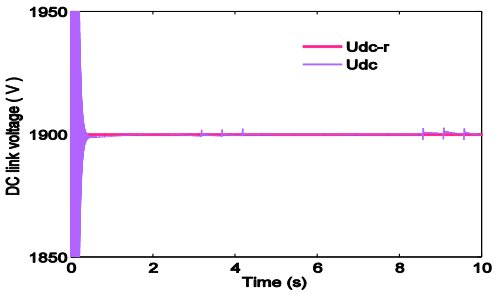

(d) *DC link voltage (V).*

Figure 12. Waveforms of WFS characteristics with PI controllers.

at the Bus 4 of the 1 MW loads (Figure 2), and it is introduced at t = 4.3s for 150 ms. Figure 13c-g and Figure 13d-h illustrate the waveforms of RMS lines ground voltage variations and a closer observation of three phase voltage at Bus 1 during the electric network fault period. RMS lines ground voltages and three phase voltage at Bus 1 clearly show the different reaction at transient states by the SMC strategy and PI regulator. According to Figure 13c-g, if using PI controllers, three phase voltage fluctuations were more severe distorted. So, PI control system is highly sensitive to external disturbances of system. Besides, the waveform of three phase voltage is easily distorted. In contrast, the system using SMC methodology is less sensitive to three phase grid short circuit fault. Figure 14 shows the difference in frequency performance between the two controlling strategies SMC and PI controller. An increase in frequency can be observed as can be seen in Figure 14(a). But, the size of the overshoot is very small. Within a short period of time, the frequency response is capable to converge to the nominal value. Consequently, the proposed strategy obviously improves the VS-WFS performances. Figure 14 shows that maximum frequency deviations are reduced from 1.34 Hz to less than 0.22 Hz with SMC, and that the fault induced frequency variations almost disappear. Also, the frequency excursion is arrested earlier in SMC. Consequently, the frequency deviations are substantially reduced during the fault. According to the simulation results, it can be seen that the proposed strategy is efficient and the control performance is acceptable.

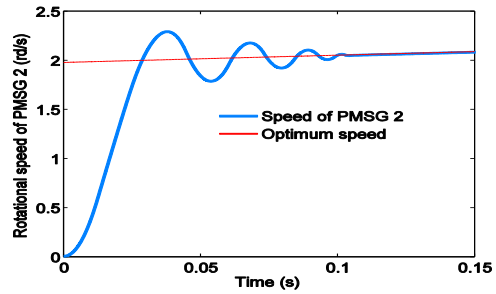

(a) Speed of PMSG2 (rd/s) for SMC.

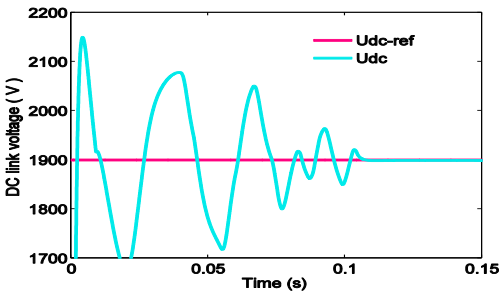

(b)

(b) DC link voltage (V) for SMC.

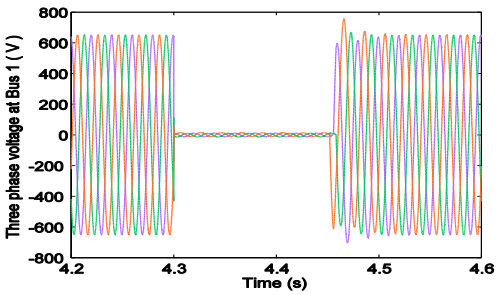

(c). Three phase voltage at Bus 1 for SMC.

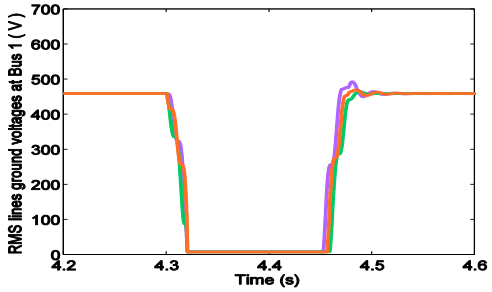

(d) RMS lines ground voltages at Bus 1 for SMC.

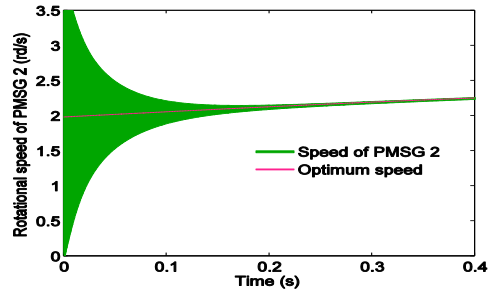

(e) Speed of PMSG2 (rd/s) for PI controllers

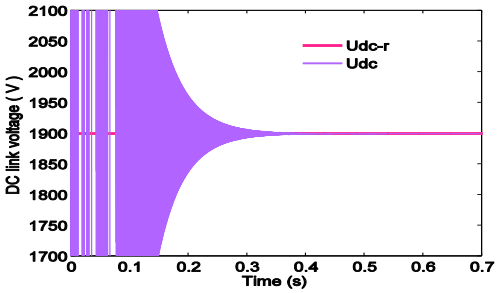

(f) DC link voltage (V) for PI controllers

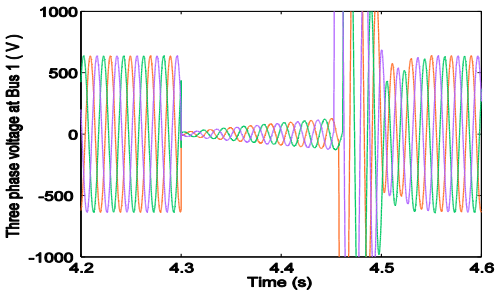

(g) Three phase voltage at Bus 1 for PI controllers.

Figure 13. Simulation results using the SMC and PI controllers.

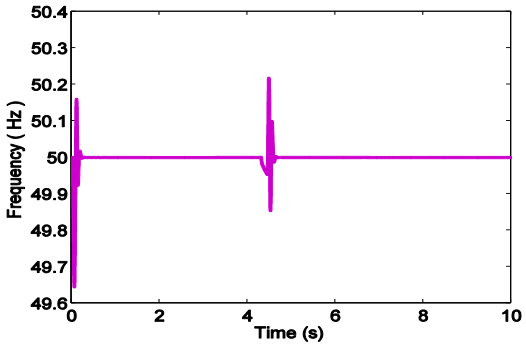

(a) *Frequency at Bus 1 for SMC*

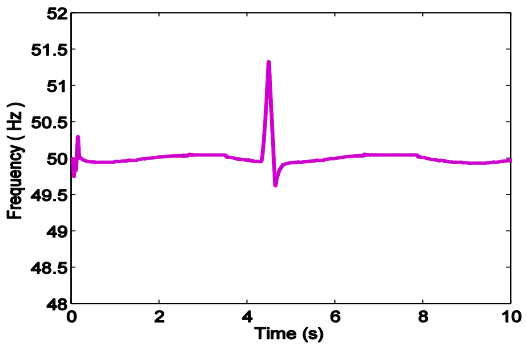

Figure 14. Frequency response of the WFS.

5. Conclusion

This study has successfully designed a SMC to handle the control of the VS-WFS. The control strategy has used Maximum Power Point Tracking (MPPT) to maximize the total generated power of VS-WFS. A pitch control scheme for the PMSG wind turbine systems has been proposed to limit the speeds of turbines and the turbine output powers at their ratings. The SMC scheme is derived in the sense of Lyapunov stability theorem, so that the system stability can be assured. The efficiency of the proposed SMC scheme is confirmed by numerical simulations for fault conditions as well as for normal working conditions, and its advantage is indicated in comparison with traditional Proportional Integral (PI) control strategy. According to the simulation results, it can be seen that the proposed strategy is efficient and the control performance is acceptable. The achievements obtained in the study are recited as follows:
(i) The successful construction of the dynamic mathematical model of VS-WFS. (ii) The successful utilisation of SM control to improve VS-WFS performance under fault conditions as well as for normal working conditions. (iii**)** The dc link voltage can be well controlled to guarantee reliable operation of the power electronic devices. (iv) Compared with the VC method, the proposed SMC scheme can provide pretty well steady-state and transient performance under the network system fault conditions.

6. References

[1]. Fengji Luo, Ke Meng, Zhao Yang Dong, Yu Zheng, Yingying Chen, Kit Po Wong, "Coordinated Operational Planning for Wind Farm With Battery Energy Storage System, "*IEEE Transactions On Sustainable Energy*, Vol. 6, No. 1, pp. 253- 262, January 2015.

[2]. Ke Ma, Marco Liserre, Frede Blaabjerg, "Comparison of Multi-MW Converters Considering the Determining Factors in Wind Power Application, "*IEEE Energy Conversion Congress and Exposition (ECCE)*, pp. 4754 – 4761, September 2013.

[3]. Y. Errami, M. Ouassaid, M. Maaroufi, "Control of Grid Connected PMSG Based Variable Speed Wind Energy Conversion System," *International Review on Modelling and Simulations (I.RE.MO.S)*, Vol. 5, No. 2, pp. 655-664, April 2012. ISSN: 1974-9821.

[4]. Y. Wang, J. Meng, X. Zhang, L. Xu, "Control of PMSG-Based Wind Turbines for System Inertial Response and Power Oscillation Damping, " *IEEE Transactions on Sustainable Energy*, Vol. 6, No. 2, pp. 565 – 574, March 2015.

[5]. Youssef Errami, Mohammed Ouassaid, Mohamed Cherkaoui, Mohamed Maaroufi, "Variable Structure Sliding Mode Control and Direct Torque Control of Wind Power Generation System Based on The PM Synchronous Generator," *Journal of ELECTRICAL ENGINEERING*, Vol. 66, No. 3, 2015, pp. 121–131. DOI: 10.1515/jee-2015-0020.

[6]. I. Jlassi, J. O. Estima, S. Khojet El Khil, N. M. Bellaaj, A. J. Marques Cardoso, " Multiple Open-Circuit Faults Diagnosis in Back-to-Back Converters of PMSG Drives for Wind Turbine Systems," *IEEE Transactions on Power Electronics,* Vol. 30, Vol. 5, pp. 2689 – 2702, May 2015.

[7]. Nuno M. A. Freire, Jorge O. Estima, António J. Marques Cardoso, "A New Approach for Current Sensor Fault Diagnosis in PMSG Drives for Wind Energy Conversion Systems," *IEEE Transactions On Industry Applications*, Vol. 50, No. 2, pp. 1206-1214, March/April 2014.

[8]. Marius Fatu, Frede Blaabjerg, Ion Boldea, "Grid to Standalone Transition Motion Sensorless Dual-Inverter Control of PMSG With Asymmetrical Grid Voltage Sags and Harmonics Filtering," *IEEE Transactions On Powers Electronics*, Vol. 29, No. 7, pp. 3463-3472, July 2014.

[9]. Errami, Y.; Maaroufi, M.; Ouassaid, M., "A MPPT vector control of electric network connected Wind Energy Conversion System employing PM Synchronous Generator," *Renewable and Sustainable Energy Conference (IRSEC)*, 2013 International, vol., no., pp.228,233, 7-9 March 2013, doi: 10.1109/IRSEC.2013.6529721.

[10]. Youssef Errami, Mohammed Ouassaid, Mohamed Maaroufi, "Optimal Power Control Strategy of Maximizing Wind Energy Tracking and different operating conditions for Permanent Magnet Synchronous Generator Wind Farm," Energy Procedia, pp. 477 – 490, Vol. 74, 2015. DOI: 10.1016/j.egypro.2015.07.732.

[11]. Frede Blaabjerg, Ke Ma, Future on Power Electronics for Wind Turbine Systems, *IEEE Journal of Emerging And Selected Topics in power Electronics*, Vol. 1, No. 3, pp. 139-152, September 2013.

[12]. Y. Errami, M. Ouassaid, M. Maaroufi, "Control of a PMSG based wind energy generation system for power maximization and grid fault conditions, " Energy Procedia, pp. 220–229, Vol. 42, 2013. doi: 10.1016/j.egypro.2013.11.022.

[13]. Jiawei Chen, Jie Chen, Chunying Gong, "On Optimizing the Aerodynamic Load Acting on the Turbine Shaft of PMSG-Based Direct-Drive Wind Energy Conversion System," *IEEE Transactions On Industrial Electronics*, Vol. 61, No. 8, pp. 4022-4031, August 2014.

[14]. Omid Alizadeh, Amirnaser Yazdani, "A Strategy for Real Power Control in a Direct-Drive PMSG-Based Wind Energy Conversion System," *IEEE Transactions On Power Delivery*, Vol. 28, No. 3, pp. 1297-1305, July 2013.

[15]. Rui Li, Dianguo Xu, "Parallel Operation of Full Power Converters in Permanent-Magnet Direct-Drive Wind Power Generation System," *IEEE Transactions On Industrial Electronics*, Vol. 60, No. 4, pp. 1619-1629, April 2013.

[16]. Dante Fernando Recalde Melo, Le-Ren Chang-Chien, "Synergistic Control Between Hydrogen Storage System and Offshore Wind Farm for Grid Operation," *IEEE Transactions On Sustainable Energy*, Vol. 5, No. 1, pp. 18-27, January 2014.

[17]. Youssef Errami, Mohammed Ouassaid, Mohamed Maaroufi, " Modelling and Optimal Power Control for Permanent Magnet Synchronous Generator Wind Turbine System Connected to Utility Grid with Fault Conditions," *World Journal of Modelling and Simulation*, Vol. 11 (2015) No. 2, pp. 123-135.
[18]. Y. Errami, M. Ouassaid, M. Maaroufi, "Control of a PMSG based wind energy generation system for power maximization and grid fault conditions, " Energy Procedia, pp. 220–229, Vol. 42, 2013. doi: 10.1016/j.egypro.2013.11.022.
[19]. Li .Shuhui, T.A Haskew, R.P. Swatloski, W. Gathings,"Optimal_and_Direct-Current Vector_Control_of_Direct-Driven_PMSG_Wind_Turbines," *IEEE Transactions on Power Electronics*, Vol. 27, No. 5, pp. 2325 – 2337, May 2012.
[20]. Y. Errami, M. Ouassaid, M. Maaroufi, "Control scheme and power maximization of permanent magnet synchronous generator wind farm connected to the electric network", *International Journal of Systems, Control and Communications (IJSCC)*, Vol. 5, No. 3/4, pp. 214 – 230, 2013.
[21]. Wang xin, Cao Mingfeng, Qiu Li, Chai Lulu, Qin Bin, "Control of Direct-drive Permanent-magnet Wind Power System Grid-Connected Using Back-to-back PWM Converter," *IEEE International Conference on Intelligent System Design and Engineering Applications*, pp. 478 – 481, January 2013.
[22]. Hamid Shariatpanah, Roohollah Fadaeinedjad, Masood Rashidinejad, " A New Model for PMSG-Based Wind Turbine With Yaw Control," *IEEE Transactions On Energy Conversion*, Vol. 28, No. 4, pp. 929-937, December 2013.
[23]. Errami, Y.; Benchagra, M.; Hilal, M.; Maaroufi, M.; M. Ouassaid, "Control strategy for PMSG wind farm based on MPPT and direct power control," *Multimedia Computing and Systems (ICMCS)*, 2012 International Conference on, vol., no., pp.1125, 1130, 10-12 May2012, doi: 10.1109/ICMCS.2012.6320210.
[24]. Thanh Hai Nguyen, Dong-Choon Lee, "Advanced Fault Ride-Through Technique for PMSG Wind Turbine Systems Using Line-Side Converter as STATCOM," *IEEE Transactions on Industrial Electronics*, Vol. 60, No. 7, pp. 2842- 2850, July 2013.
[25]. A. Harrouz, A. Benatiallah, O. Harrouz, "Direct Power Control of a PMSG Dedicated to Standalone Wind Energy Systems, " *IEEE Eighth International Conference and Exhibition on Ecological Vehicles and Renewable Energies (EVER)*, pp. 1 – 5, March 2013.
[26]. Amir hossein Rajaei, Mustafa Mohamadian, Ali Yazdian Varjani, "Vienna-Rectifier-Based Direct Torque Control of PMSG for Wind Energy Application," *IEEE Transactions on Industrial Electronics*, Vol. 60, No. 7, pp. 2919-2929, July 2013.
[27]. Errami, Y., M. Benchagra, M. Hillal, M. Ouassaid, M. Maaroufi, "MPPT Strategy and Direct Torque Control of PMSG Used for Variable Speed Wind Energy Conversion System," *International Review on Modelling and Simulations (I.RE.MO.S)*, Vol. 5, No. 2, pp. 887- 898, April 2012. ISSN: 1974-9821.
[28]. Zhe Zhang, Vue Zhao, Wei Qiao, Liyan Qu, "A Discrete-Time Direct-Torque and Flux Control for Direct-Drive PMSG Wind Turbines," *IEEE Industry Applications Society Annual Meeting*, pp. 1 – 8, October 2013.
[29]. A. Harrouz, A. Benatiallah, A. Moulay ali, O. Harrouz, "Control of Machine PMSG Dedicated to the Conversion of Wind Power Off-Grid," *IEEE International Conference on Power Engineering, Energy and Electrical Drives Istanbul*, pp. 1729 - 1733 , May 2013.
[30]. Errami, Y.; Maaroufi, M.; Cherkaoui, M.; Ouassaid, M., "Maximum power point tracking strategy and direct torque control of permanent magnet synchronous generator wind farm," in *Complex Systems (ICCS), 2012 International Conference* on, vol., no., pp.1-6, 5-6 Nov. 2012. doi: 10.1109/ICoCS.2012.6458520.
[31]. Jianhu Yan, Heyun Lin, Yi Feng, Xun Guo, Yunkai Huang, Z.Q. Zhu, "Improved sliding mode model reference adaptive system speed observer for fuzzy control of direct-drive

permanent magnet synchronous generator wind power generation system, " *IET Renewable Power Generation*, Vol. 7, No. 1, pp. 28–35, 2013.
[32]. J. E Slotine and Li W, "Applied Nonlinear Control," Prentice Hall, Englewood Cliffs, New Jersey, 1991.
[33]. Utkin V. I, "Sliding mode control design principles and applications to electrical drives," *IEEE Transactions on Industrial Electronics*, vol. 40, No. 1, pp. 23 – 36, February 1993.
[34]. C. Evangelista, P. Puleston, F. Valenciaga, L. M. Fridman, "Lyapunov-Designed Super Twisting Sliding Mode Control for Wind Energy Conversion Optimization," *IEEE Transactions on Industrial Electronics*, Vol. 60, No. 2, pp. 538 -545, February 2013.
[35]. Shihua Li, Haibo Du, Xinghuo Yu, "Discrete-time terminal sliding mode control systems based on Euler's discretization," *IEEE Transactions on Automatic Control*, Vol. 59, No. 2, pp. 546 - 552, February 2014.
[36]. Carolina Evangelista, Fernando Valenciaga, and Paul Puleston, "Active and Reactive Power Control for Wind Turbine Based on a MIMO 2-Sliding Mode Algorithm With Variable Gains," *IEEE Transactions on Energy Conversion*, Vol. 28, No. 3, pp. 682-689, September 2013.
[37]. Y.Errami, M.Hilal M.Benchagra, M.Ouassaid, M.Maaroufi "Nonlinear Control of MPPT and Grid Connected for Variable Speed Wind Energy Conversion System Based on the PMSG" *Journal of Theoretical and Applied Information Technology*, Vol. 39, No.2, pp.205- 217, May 2012.
[38]. Ana Susperregui, Miren Itsaso Martinez, Gerardo Tapia, Ionel Vechiu, "Second-order sliding-mode controller design and tuning for grid synchronisation and power control of a wind turbine-driven doubly fed induction generator," *IET Renewable Power Generation*, Vol. 7, No. 5, pp. 540 – 551, September 2013.
[39]. Shuai Xiao, Geng Yang, Hua Geng, "Individual Pitch Control Design of Wind Turbines for Load Reduction Using Sliding Mode Method," *IEEE International Energy Conversion Congress and Exhibition ECCE Asia Downunder (ECCE Asia)*, pp. 227 – 232, June 2013.
[40]. Bidyadhar Subudhi, Pedda Suresh Ogeti, "Sliding Mode Approach to Torque and Pitch Control for a Wind Energy System," *IEEE India Conference (INDICON)*, pp. 244 – 250, December 2012.
[41]. Miren Itsaso Martinez, Ana Susperregui, Gerardo Tapia, Lie Xu, "Sliding-mode con-trol of a wind turbine-driven double-fed induction generator under non-ideal grid volt-ages," *IET Renewable Power Generation*, Vol. 7, No. 4, pp. 370 – 379, July 2013.
[42]. Bin Chen, Yong Feng, Minghao Zhou, "Terminal Sliding-Mode Control Scheme for Grid-side PWM Converter of DFIG-based Wind Power System," *IEEE Conference of the Industrial Electronics Society (IECON)*, pp. 8014 – 8018, November 2013.
[43]. B.Bouaziz, F.Bacha, "Direct Power Control of Grid-Connected Converters Using Sliding Mode Controller," *IEEE International Conference on Electrical Engineering and Software Applications (ICEESA)*, pp. 1-6, March 2013.
[44]. M. Benchagra, M. Hilal, Y. Errami, M. Ouassaid, M. Maaroufi, "Modeling and Control of SCIG based variable-Speed with Power Factor Control," *International Review on Modelling and Simulations (IREMOS)*, Vol. 4, No.3, pp. 1007-1014, June 2011. ISSN: 1974-9821.
[45]. Errami, Y.; Maaroufi, M.; Ouassaid, M., "Modelling and control strategy of PMSG based variable speed wind energy conversion system," in *Multimedia Computing and Systems (ICMCS)*, 2011 International Conference on, vol., no., pp.1-6, 7-9 April 2011. doi: 10.1109/ICMCS.2011.5945736.
[46]. Feifei Bu, Yuwen Hu, Wenxin Huang, Shenglun Zhuang, Kai Shi, "Wide-Speed-Range-Operation Dual Stator-Winding Induction Generator DC Generating System for Wind Power Applications," *IEEE Transactions On Power Electronics*, Vol. 30, No. 2, pp. 561-573, February 2015.

[47]. Benchagra, M.; Hilal, M.; Errami, Y.; Maaroufi, M.; Ouassaid, M., "Nonlinear control of DC-bus voltage and power for Voltage Source Inverter," in *Multimedia Computing and Systems (ICMCS)*, 2012 International Conference on, vol., no., pp.1049-1054, 10-12 May 2012 doi: 10.1109/ICMCS.2012.6320130.

[48]. M. Hilal, M. Benchagra, Y. Errami, M. Maaroufi, "Fuzzy Power Control For Doubly Fed Induction Generator Based Wind Farm", *Journal of Theoretical and Applied Information Technology (JATIT)*, Vol. 43, No. 2, pp 321 – 330, September 2012.

7. Appendix: Parameters of the system under study

Table 1. Parameters of The Power Synchronous Generators

Parameter	Value
P_r rated power	2 (MW)
ω_m rated mechanical speed	2.57 (rd/s)
R stator resistance	0.008(Ω)
L_s stator d-axis inductance	0.0003 (H)
ψ_f permanent magnet flux	3.86 (wb)
p_n pole pairs	60

Table 2. Parameters of The turbine

Parameter	Value
ρ the air density	1.08kg/m^3
A area swept by blades	4775.94 m^2
v_n base wind speed	12.4 m/s

Youssef Errami received his Agrégation Diploma in Electrical Engineering from Ecole Normale Supérieure de l'Enseignement Technique (ENSET), Rabat, Morocco in 2001 and DESS from Laboratory of Physical, Chouab Doukkali University, Eljadida- Morocco, in 2005. In 2009, he joined Electric Machines Laboratory at the Department of Electrical Engineering of Mohammadia School's of Engineers, Rabat, Morocco. In 2013, he received his PhD in Electrical Engineering. He is currently a Professor at Faculty of Science, Chouaib Doukkali University, Eljadida, Morocco. Prof. Errami is member of Laboratory: Electronics, Instrumentation and Energy (LEIE)- Team: Exploitation and Processing of Renewable Energy (EPRE)- Physical Department, Faculty of Sciences. His research interests are in the areas of renewable energy, power electronics systems, electric drives and power systems. He is a member of the IEEE.

Abdellatif Obbadi was born in El Jadida, Morocco. He received this diploma in Electrical Engineering from the Ecole Normal Superior of Technical Education (ENSET), Mohammedia, Morocco in 1993, and the DESA degree in measurement instrumentation and control from the Faculty of Science University Chouaib Doukkali EI Jadida, Morocco in 1999. He received his Ph.D. and H.D.R degree from the Faculty of Science University Chouaib Doukkali EI Jadida, Morocco respectively in 2007 and 2016. He is currently working toward his Ph.D. degree in the Laboratory of Electronics, Instrumentation and Energy (LEIE), Team: Exploitation and Processing of Renewable Energy (EPRE) Faculty of Science University Chouaib Doukkali Department of Physics EI Jadida,

Morocco. His current research interests include photovoltaic system modeling, modeling of dc–dc converters, maximum power point tracking of photovoltaic power, and grid integration of renewable energy sources.

Smail Sahnoun is currently research professor at the distinguished Professor rank at the Chouaib Doukkali University-Eljadida, Morocco. He is director of the Laboratory of Electronics, Instrumentation and Energy (LEIE)- Faculty of Science- University Chouaib Doukkali- Department of Physics-EI Jadida, Morocco. His main research interests are renewable energy and non-destructive thermal control. He is author of several scientific articles.

Mohammed Ouassaid received his Diplôme d'agrégation in Electrical Engineering from Ecole Normal Supérieur de l'Enseignement Technique,Rabat, in 1999, and MScA and PhD degrees in Electrical Engineering from Ecole Mohammadia d'Ingénieur, Université Mohamed V, Rabat, Morocco, in 2002 and 2006, respectively. He is currently a Professor at Mohammadia School's of Engineers, University Mohammed V, Rabat, Morocco. His research interests are electric drives, power electronics, power systems
and renewable energy. He is a member of the IEEE.

Mohamed Maaroufi received his Diplôme d'ingénieur d'état degree from the Ecole Mohammadia, Rabat, Morocco, in 1979 and PhD degrees from the Liége University, Belgium, in 1990 in Electrical Engineering. In 1990, he joined the Department of Electrical Engineering, Ecole Mohammadia, Rabat, Morocco, where he is currently Professor and University Research Professor. His current research interests include electrical network, renewable energy, motor drives and power systems.